



## RESEARCH ARTICLE

10.1002/2015GC005909

### Special Section:

Magnetism From Atomic to Planetary Scales: Physical Principles and Interdisciplinary Applications in Geo- and Planetary Sciences

### Key Points:

- FORC diagrams are powerful for unmixing magnetic domain states
- PCA represents FORC data according to natural variability in data sets
- Samples are recast as linear combinations of end-member FORCs in PCA space

### Supporting Information:

- Supporting Information S1
- Supporting Information S2
- Movie S1
- Movie S2

### Correspondence to:

I. Lascu,  
il261@cam.ac.uk

### Citation:

Lascu, I., R. J. Harrison, Y. Li, J. R. Muraszko, J. E. T. Channell, A. M. Piotrowski, and D. A. Hodell (2015), Magnetic unmixing of first-order reversal curve diagrams using principal component analysis, *Geochem. Geophys. Geosyst.*, *16*, 2900–2915, doi:10.1002/2015GC005909.

Received 12 MAY 2015

Accepted 12 AUG 2015

Accepted article online 14 AUG 2015

Published online 5 SEP 2015

## Magnetic unmixing of first-order reversal curve diagrams using principal component analysis

Ioan Lascu<sup>1</sup>, Richard J. Harrison<sup>1</sup>, Yuting Li<sup>1</sup>, Joy R. Muraszko<sup>1</sup>, James E. T. Channell<sup>2</sup>, Alexander M. Piotrowski<sup>1</sup>, and David A. Hodell<sup>1</sup>

<sup>1</sup>Department of Earth Sciences, University of Cambridge, Cambridge, UK, <sup>2</sup>Department of Geological Sciences, University of Florida, Gainesville, Florida, USA

**Abstract** We describe a quantitative magnetic unmixing method based on principal component analysis (PCA) of first-order reversal curve (FORC) diagrams. For PCA, we resample FORC distributions on grids that capture diagnostic signatures of single-domain (SD), pseudosingle-domain (PSD), and multidomain (MD) magnetite, as well as of minerals such as hematite. Individual FORC diagrams are recast as linear combinations of end-member (EM) FORC diagrams, located at user-defined positions in PCA space. The EM selection is guided by constraints derived from physical modeling and imposed by data scatter. We investigate temporal variations of two EMs in bulk North Atlantic sediment cores collected from the Rockall Trough and the Iberian Continental Margin. Sediments from each site contain a mixture of magnetosomes and granulometrically distinct detrital magnetite. We also quantify the spatial variation of three EM components (a coarse silt-sized MD component, a fine silt-sized PSD component, and a mixed clay-sized component containing both SD magnetite and hematite) in surficial sediments along the flow path of the North Atlantic Deep Water (NADW). These samples were separated into granulometric fractions, which helped constrain EM definition. PCA-based unmixing reveals systematic variations in EM relative abundance as a function of distance along NADW flow. Finally, we apply PCA to the combined data set of Rockall Trough and NADW sediments, which can be recast as a four-EM mixture, providing enhanced discrimination between components. Our method forms the foundation of a general solution to the problem of unmixing multicomponent magnetic mixtures, a fundamental task of rock magnetic studies.

### 1. Introduction

Quantifying magnetic particle ensembles in rocks and sediments is a fundamental task in virtually all paleomagnetic and environmental magnetic studies. The magnetic state of a particle is highly sensitive to its size and shape, changing from superparamagnetic (SP) to stable single domain (SD) to pseudosingle-domain (PSD) and finally to multidomain (MD) as the particle size increases from a few tens of nanometers to several tens of micrometers. Rock and mineral magnetists have devised an extensive “toolbox” of magnetic methods designed to reveal the presence of different magnetic states within a sample [Robertson and France, 1994; Kruiver *et al.*, 2001; Heslop *et al.*, 2002; Egli, 2004; Dunlop and Carter-Stiglitz, 2006; Heslop and Dillon, 2007; Lascu *et al.*, 2010; Heslop and Roberts, 2012a, 2012b; Heslop, 2015]. The problem is that most natural samples contain a complex, multicomponent mixture of different magnetic phases with a wide range of particle sizes derived from a variety of possible sources. The convolution of magnetic signals from these different mineral populations results in complex bulk magnetic signatures, which reflect the totality of factors that have influenced the history of the magnetic ensemble, e.g., crystallization or depositional conditions, weathering and alteration, provenance, transport processes, climatic and environmental variability, etc. While current techniques are successful at revealing qualitative trends in behavior, they do not lend themselves readily to obtaining an unambiguous quantitative unmixing of the SP, SD, PSD, and MD fractions present.

First-order reversal curve (FORC) diagrams provide a potential solution to this problem. FORCs are an advanced method of characterizing the magnetic properties of a sample and are highly sensitive to variations in grain size. This sensitivity derives from the strong variation in magnetic domain state with increasing grain size, which manifests itself in FORC diagrams as a gradual change from horizontal to vertical spreading of the FORC distribution. FORCs allow researchers to fingerprint domain states, extract coercivity distributions for these domain states, and detect geometry-specific magnetostatic interaction fields rather

unambiguously [Pike et al., 1999; Roberts et al., 2000, 2014]. FORC distributions can also be simulated using well-established physical models of magnetic behavior [Harrison and Lascu, 2014]. In addition, recent developments allow the quantification of diagnostic FORC signatures, such as those of noninteracting SD particles and magnetosome (magnetite crystal produced by magnetotactic bacteria) chains, in particular the so-called “central ridge,” a narrow positive feature along the horizontal axis of a FORC diagram [Egli et al., 2010; Egli, 2013; Ludwig et al., 2013; Heslop et al., 2014].

A further development toward quantification of FORC diagram signatures has been proposed by Heslop et al. [2014], who employed principal component analysis (PCA) on extracted central ridge coercivity distributions to highlight intersequence and intrasequence variability in magnetosome-rich ocean sediment sequences. However, focusing solely on central ridges means ignoring other SD signatures, as well as non-SD contributions to the FORC diagram, which are often the most abundant components in geological samples. In this study, we perform PCA on a subset of the FORC space that encompasses all significant magnetic signatures and use the PCA space as the canvas for developing a physically-constrained empirical unmixing model [Heslop, 2015]. PCA provides an objective and robust statistical framework for unmixing, because it represents data variability as a linear combination of  $n$  significant principal components (PCs) that are derived purely on the basis of natural variations contained within the data set, unbiased by user input [Abdi and Williams, 2010; Wold et al., 1987]. With appropriate data normalization, the  $n$ -dimensional PCA space can then be used to define a mixing region for a system with  $n + 1$  end-members (EMs), represented here by known domain state FORC signatures, which are assumed to be effectively unchanging throughout the sample set. By using PCA, we allow for the freedom to constrain the EMs to adhere to a set of well-defined criteria that include the requirement that model EMs correspond to physically realistic domain state FORC signatures. To impose constraints on the EMs, we use samples characterized by a limited number of domain state signatures. To ensure this, the samples have been either selected from sedimentary environments with a limited number of magnetic components, or have been physically separated in the laboratory to produce narrow grain size fractions. We test binary, ternary, and quaternary mixtures and demonstrate how the method provides the foundation of a general solution to the problem of unmixing multicomponent magnetic ensembles.

## 2. Methods

### 2.1. Samples and FORC Acquisition

The samples used in this study are from North Atlantic sediment cores (Table 1). The first batch of samples is from giant piston core MD04–2822, recovered by the RV Marion Dufresne from the distal margin of the Barra Fan in the Rockall Trough, NW of the British Isles [Hibbert et al., 2010]. A 1.5 m core section spanning the late Pleistocene-Holocene transition was sampled contiguously at 2 cm intervals and the bulk sediment was used for FORC acquisition. A second batch of samples comes from two surface cores (SHAK-06-5M-C and SHAK-10-9M-F) collected from the Iberian Continental Margin using a Bowers and Connelly multiple corer during expedition 89 of the RSS James Cook. The cores (~30 cm long) were sampled contiguously at 1 cm intervals, and selected samples (every cm in the upper 10 cm, and every 2 or 3 cm in the lower 20 cm) were used for FORC acquisition. A third batch of samples, used for the analysis of granulometric fractions, is from piston cores collected during Cruise 159 of the RSS Charles Darwin along the western margin of the Atlantic. The cores are located along the Deep Western Boundary Current (DWBC), a geostrophic current which carries Denmark Strait Overflow Water and Iceland-Scotland Overflow Water (precursors of North Atlantic Deep Water) from their formation sites in the North Sea southward past Iceland, along the southern

Greenland margin and into the Labrador Sea and North American margin. We focused on late Holocene sediments from the tops of the three cores: RAPiD 10-6B (R10), RAPiD 29-18B (R29), and RAPiD 41-30B (R41). The silt and clay fractions were separated from the sand fraction by washing through a 63  $\mu\text{m}$  sieve with deionized water. The <63  $\mu\text{m}$  fraction was treated successively with acetic acid to dissolve carbonates, hydroxylamine

**Table 1.** Name, Location, and Water Depth at Retrieval Site for the Studied Cores

Core Name	Latitude (N)	Longitude (W)	Water Depth (m)
RAPiD 10-6B (R10)	62°58.39'	17°35.75'	1249
RAPiD 29-18B (R29)	58°48.01'	44°51.82'	2145
RAPiD 41-30B (R41)	50°42.65'	49°42.82'	1271
MD04–2822	56°50.54'	11°22.96'	2344
SHAK-06-5M-C	37°33.68'	10°08.53'	2645
SHAK-10-9M-F	37°50.50'	09°30.65'	1127

hydrochloride to leach amorphous Fe-Mn oxides, and sodium carbonate to remove silica. The remaining siliclastic sediment was gravity settled in sedimentation cylinders, and six size fractions were separated using Stokes' law: a clay-sized fraction ( $<4 \mu\text{m}$ ) and five silt-sized fractions (4–10, 10–20, 20–30, 30–40, and 40–63  $\mu\text{m}$ ). The grain-size distribution of each size fraction was measured using a Coulter Counter Multisizer three particle-size analyzer, confirming that the settling produced the grain size expected (with some overlap between neighboring fractions). All sediment samples were dried and packed in gel caps. FORCs were acquired at field increments of 1–2 mT using Princeton Measurements Corporation vibrating sample magnetometers at the University of Cambridge and University of Florida.

**2.2. Principal Component Analysis and Unmixing Model**

Raw FORC data were imported in FORCinel [Harrison and Feinberg, 2008] and processed using the VARIFORC variable smoothing algorithm [Egli, 2013]. For each sample, we extracted a rectangular region of FORC space, capturing the horizontal and vertical range of signals associated with the domain states present in the FORC diagram. The selected region was down sampled to a regular grid of points with a typical resolution of 2–5 mT (Figure 1). Down-sampling performs two important functions: it reduces the total number of data points  $D$  needed to define each FORC diagram, hence minimizing the processing and memory requirements of the PCA, and it allows FORCs acquired using different measurement parameters to be combined

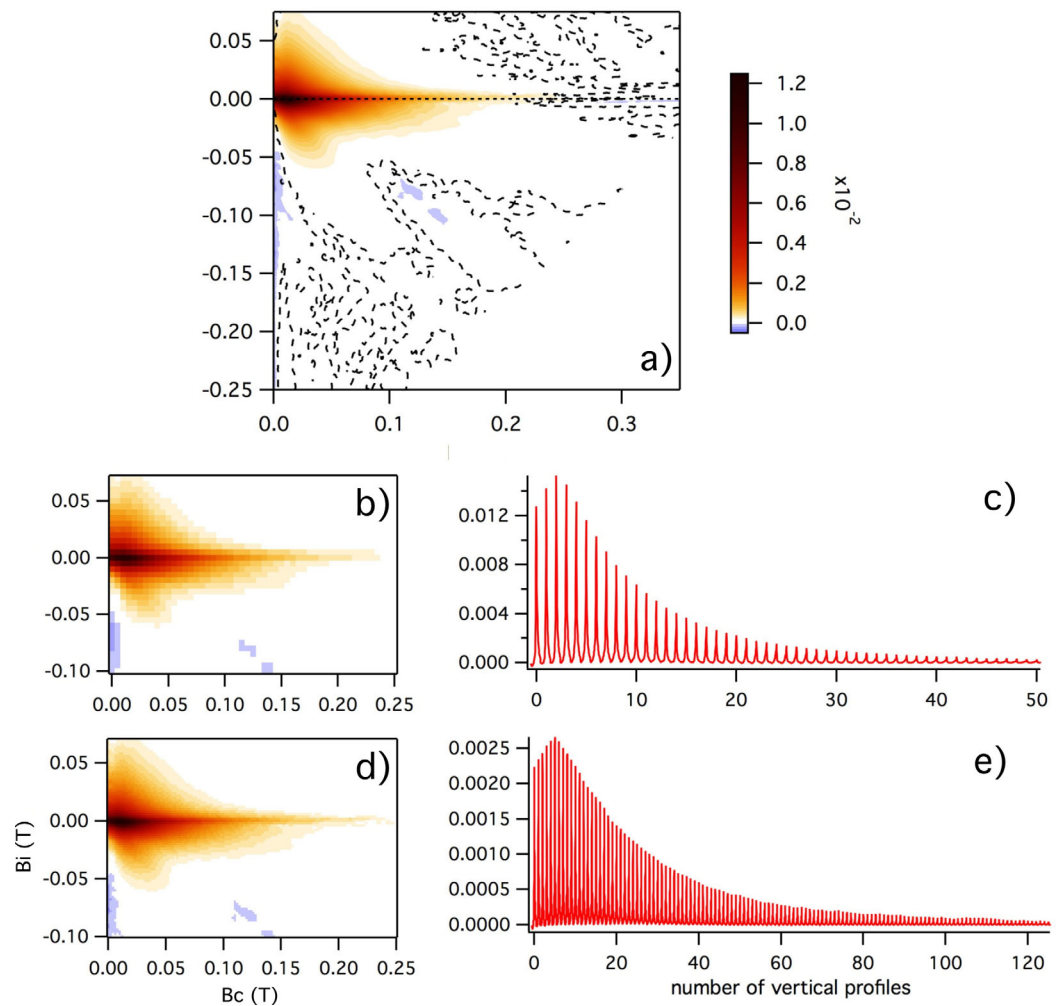


**Figure 1.** Data selection for principal component analysis (PCA). (a) Processed FORC diagram. Dashed line (here and in subsequent FORC diagrams) indicates regions of the FORC distribution significant at the 0.05 level [Heslop and Roberts, 2012c]. Color-scale units for all data FORCs are  $\text{Am}^2/\text{T}^2$ ; (b) resampled FORC data on a 5 mT resolution rectangular grid; (c) array containing the data from grid in Figure 1b as a succession of 51 vertical profiles (taken every 5 mT from 0 to 250 mT); (d) resampled FORC data on a 2 mT resolution rectangular grid; (e) array containing the data from grid in Figure 1d as a succession of 126 vertical profiles (taken every 2 mT from 0 to 250 mT). Data in Figures 1b–1e were normalized to sum to unity.

in a single analysis. Identical measurement and smoothing parameters used in data acquisition and processing are not critical, and may not even be justified in the case of very different samples (e.g., SD dominated versus MD dominated). What is important is that the combination of measurement resolution and smoothing factor (SF) employed be consistent among samples used in the analysis. Grid resolutions of 2–5 mT are sufficient for routine high-resolution protocols (i.e., 0.5–1.5 mT field increments, SF < 4). However, we have noticed a significant dropoff in quality for lower-grid resolutions (>5 mT), with computing time improving only marginally. On the other hand, down-sampling resolutions <2 mT are computationally expensive, but are only necessary for special cases where ultrahigh-resolution measurement protocols (<0.5 mT field increments) are justified.

Each down-sampled FORC grid was rearranged in one dimension, as a vector ( $\mathbf{F}_i$ ) of length  $D$ , organized as a succession of vertical profiles (Figures 1c and 1e).  $\mathbf{F}_i$  is normalized to the sum of its values, which results in the FORC data sets summing to unity:

$$\sum_{j=1}^D \mathbf{F}_i(j) = 1 \tag{1}$$

The summation to a constant is essential to the model, as it provides the basis for employing  $n + 1$  EMs in the unmixing, which can be represented in the  $n$ -dimensional PC space.

PCA is a multivariate statistical analysis method applicable to data sets comprising observations described by several intercorrelated variables, with the result of maximizing the variables' covariance through solving an eigenvalue problem [Woocay and Walton, 2008]. Hence, data from all samples were combined in a master matrix, with each row containing the data for one sample,  $i$  (i.e., the observations), and each column containing all the data for one pair of ( $B_c, B_j$ ) FORC coordinates,  $j$  (i.e., the intercorrelated variables). The vector containing the mean values of each column,  $\mathbf{A}$ , was subtracted from all  $\mathbf{F}_i$  vectors to center the data. PCA was performed via singular value decomposition on the covariance matrix of the centered data, using the built-in function in Igor Pro 6.36, which follows the operations and procedures described by Malinowski [1991].

PCA represents a transformation of the original correlated variables to new orthogonal (uncorrelated) variables (i.e., the PCs), which are parallel to the eigenvectors of the covariance matrix, and are constructed from linear combinations of the original variables. Each PC explains, in a successively decreasing residual manner, data variability not accounted for by the previous PC, i.e., the greatest mode of data variability is projected onto the first PC, the second greatest mode of variability is projected onto the second PC, etc. The number  $n$  of PCs considered should be the minimum necessary for most of the data variability to be explained, while offering a meaningful framework for interpreting the data in a geological context [Heslop and Roberts, 2012a]. In the data sets analyzed here,  $n \leq 3$ , with the first PC explaining ~70% of the variability in the case of binary mixtures, and all considered PCs explaining >90% of the variability in the case of mixtures of more than two EMs. PC scores for each sample,  $S_i^k$ , were calculated as dot products of the resulting loading vectors,  $\mathbf{L}^k$ , and the centered data for each sample (the superscript  $k$  denotes the specific PC being considered). A low-rank approximation to the FORC diagram of any given sample,  $\mathbf{F}'_i$ , can be constructed from the scores of the selected subset of PCs and their corresponding loading vectors:

$$\mathbf{F}'_i = \mathbf{A} + \sum_{k=1}^n S_i^k \mathbf{L}^k \tag{2}$$

This approximation is a relatively noise-free version of the original FORC diagram, with most of the noise being contained in the higher rank PCs, which are not statistically significant. Thus, subtracting  $\mathbf{F}'_i$  from  $\mathbf{F}_i$  allows for the computation of the FORC residuals. The root mean square (RMS) of the residuals can be employed to detect outlier samples in PCA space, which may be detrimental to the estimation of the unmixing model [Heslop, 2015]. The unmixing is performed within the  $n$ -dimensional PC score space. Equation (2) allows synthetic FORC diagrams to be constructed at any point in the score space. We identify  $n + 1$  EMs that (a) define a subregion of the PC space enclosing all sample scores (except for outliers detected by residual analysis) and (b) correspond to physically plausible FORC diagrams, that comprise, where possible, the signature of only one domain state. By "physically plausible" we mean that the constructed FORC diagram for each EM should correspond to an achievable FORC geometry based on knowledge of the



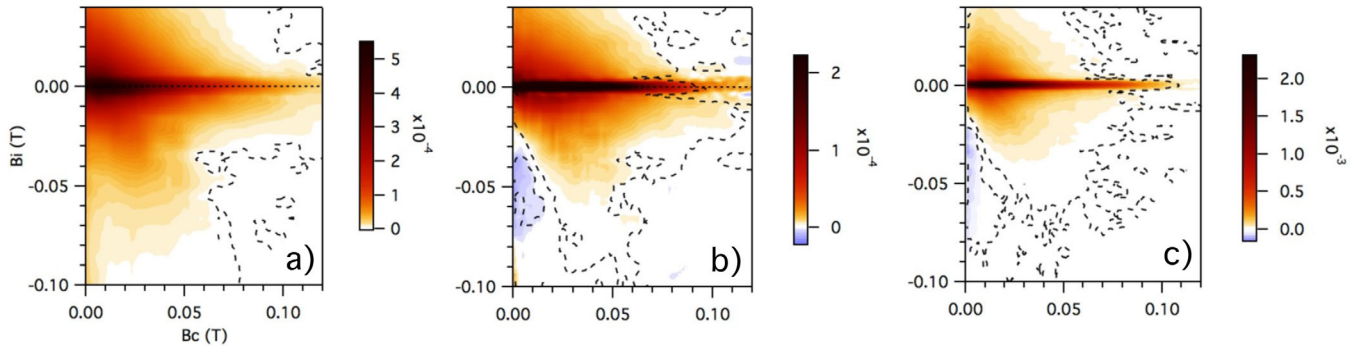


Figure 2. Typical FORC diagrams of (a) Late Glacial and (b) early Holocene sediments from Rockall Trough, and of recent sediments from (c) the Iberian Margin shelf.

magnetic mineralogy and the principles of physical modeling [Harrison and Lascau, 2014]. To perform the unmixing, the FORC diagram of each sample is recast as a linear combination of the EMs:

$$\mathbf{F}'_i = \sum_{l=1}^{n+1} f'_l \mathbf{F}^l \tag{3}$$

$$\sum_{l=1}^{n+1} f'_l = 1 \tag{4}$$

where  $\mathbf{F}^l$  is the FORC diagram of the  $l$ th EM being considered and  $f'_l$  is the proportion of that EM contributing to the sample ( $f'_l \in [0,1]$ ). Substituting equation (4) into equation (3) and equating with equation (2) leads to a set of  $n$  simultaneous equations that can be solved to obtain  $f'_l$ :

$$S_i^k = \sum_{l=1}^{n+1} f'_l S_i^k \tag{5}$$

where  $k = 1$  to  $n$ .

### 3. Results

#### 3.1. FORC Diagrams

The FORC diagrams of samples from core MD04–2822 in the Rockall Trough show a mix of fine and coarse grain signatures (Figures 2a and 2b). The overall coarsest samples are Late Glacial and are a mix of coarse PSD and fine MD (lower peak coercivity, spreading of contours about the horizontal axis, a positive lobe in lower half of the diagram) magnetite (Figure 2a), while the finest grained samples are from the early Holocene and comprise SD (higher peak coercivity, central ridge along horizontal axis, area of negative values next to the vertical axis) and PSD magnetite (Figure 2b). The FORC diagrams of the Iberian Margin samples are a mix of SD and fine PSD grains (see typical sample in Figure 2c).

The FORC diagrams of the RAPiD samples are shown in Figures 3–5. The granulometric fractions are shown in order of grain size, from finest to coarsest (a–f), with the treated unseparated  $<63 \mu\text{m}$  fraction in g. For core R10 the bulk untreated sample is shown for comparison (Figure 3h). Qualitatively, there is very little difference between the bulk sediment and the treated 0–63  $\mu\text{m}$  fraction, implying that the chemical treatments, especially leaching to remove Fe–Mn oxides, have not resulted in the dissolution of magnetic grains and that the sand fraction ( $>63 \mu\text{m}$ ), which is composed predominantly of calcite foraminifera, contributes very little to the sediment magnetism. Quantitatively, the two FORC diagrams have very similar PC scores (Figure 9), which means that the 0–63  $\mu\text{m}$  fraction is representative of the magnetic properties of the bulk sediment.

Core R10, which is located just south of Iceland, has the finest grained signature of the three cores, exhibiting a combination of SD and PSD (vertical spreading of contours, a positive lobe in lower half of the diagram at coercivities  $<100$  mT, paired with an area of negative values to the right of the lobe) features, with

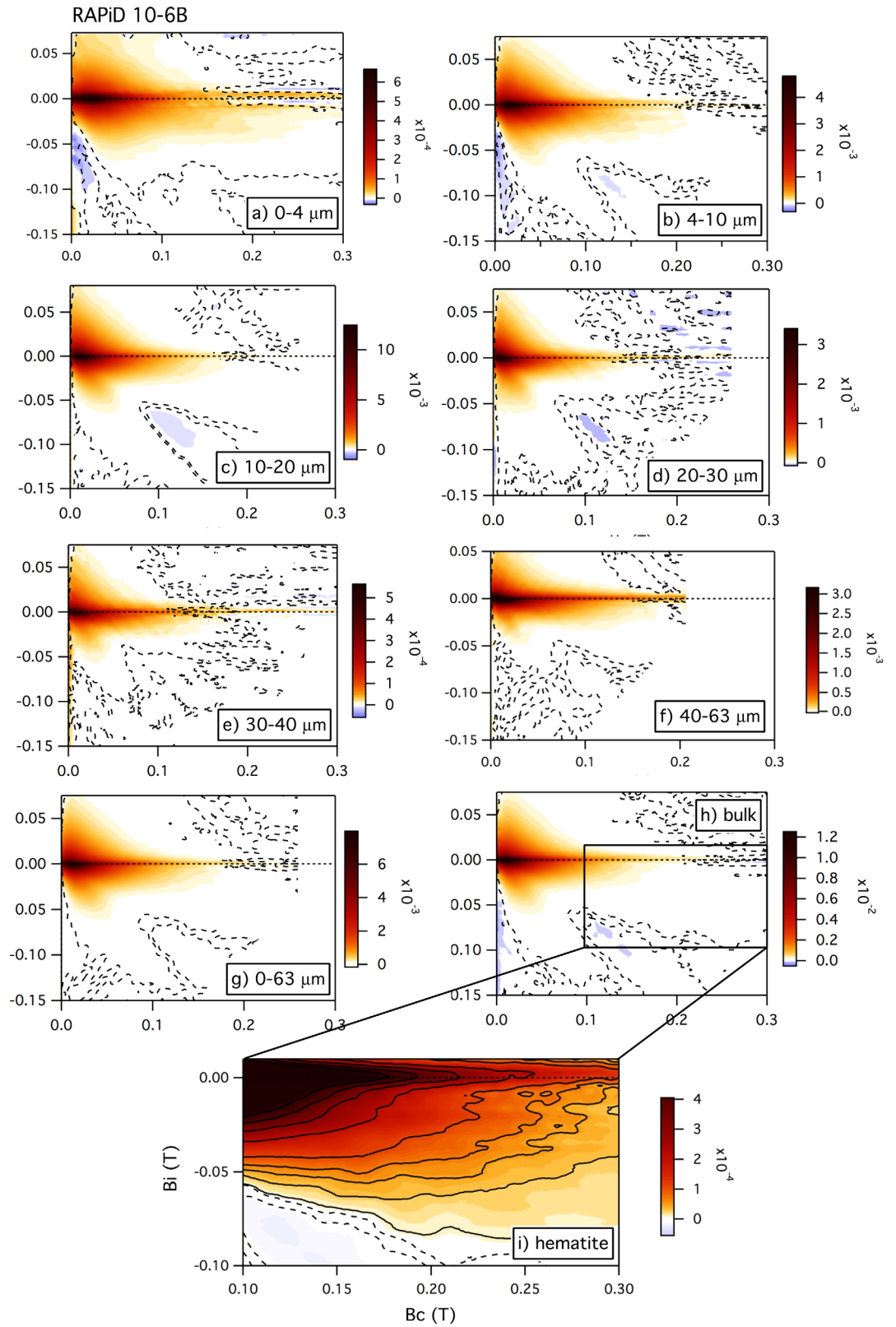


**Figure 3.** (a–f) FORC diagrams of individual particle size fractions and (g) unseparated treated sediment from Iceland-proximal core R10. (h) Untreated bulk sample is shown for comparison. Hematite signature is detailed in Figure 3i using modified color scale.

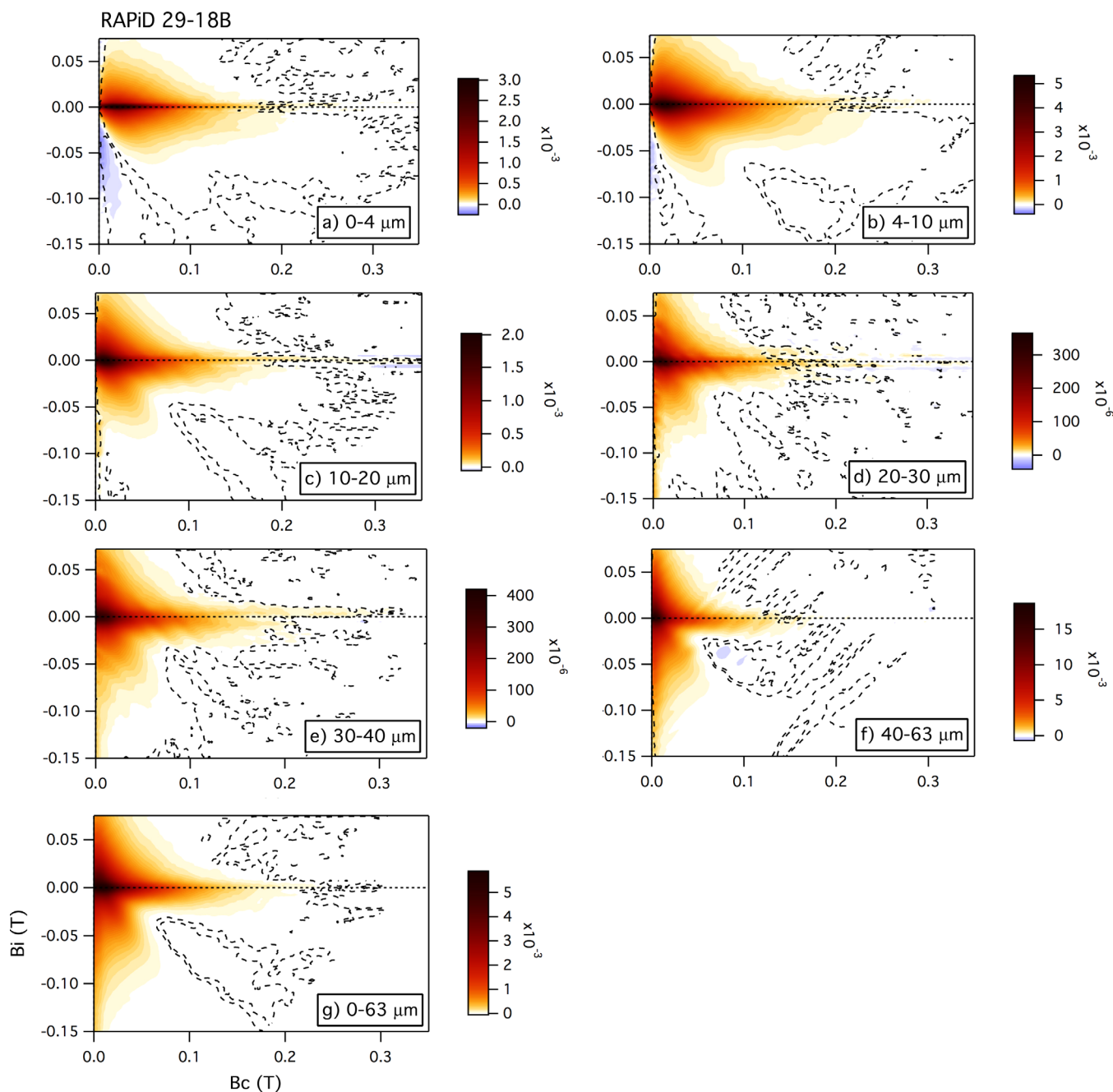


**Figure 4.** (a–f) FORC diagrams of individual particle size fractions and (g) unseparated treated sediment from Greenland-proximal core R29.

an added contribution from hematite (Figure 3h). The hematite signature can be seen as the statistically significant lobe below the horizontal axis at coercivities >100 mT (Figures 3h and 3i). In the individual size fractions, the hematite is well represented in the clay and fine silts (Figures 3a–3c), has a decreased contribution in the medium silt fractions (Figures 3d and 3e), and, interestingly, increases in the coarsest silt fraction (Figure 3f).

Core R29, located just south of Greenland, has a coarser bulk signature than R10 and smaller hematite contribution (Figure 4g). The clay fraction is characterized by a combination of SD and PSD features. Lower peak coercivity, increased vertical spreading, development of a lobe in the lower half of the diagram at coercivities <100 mT, together with the disappearance of the negative region left of the lobe,

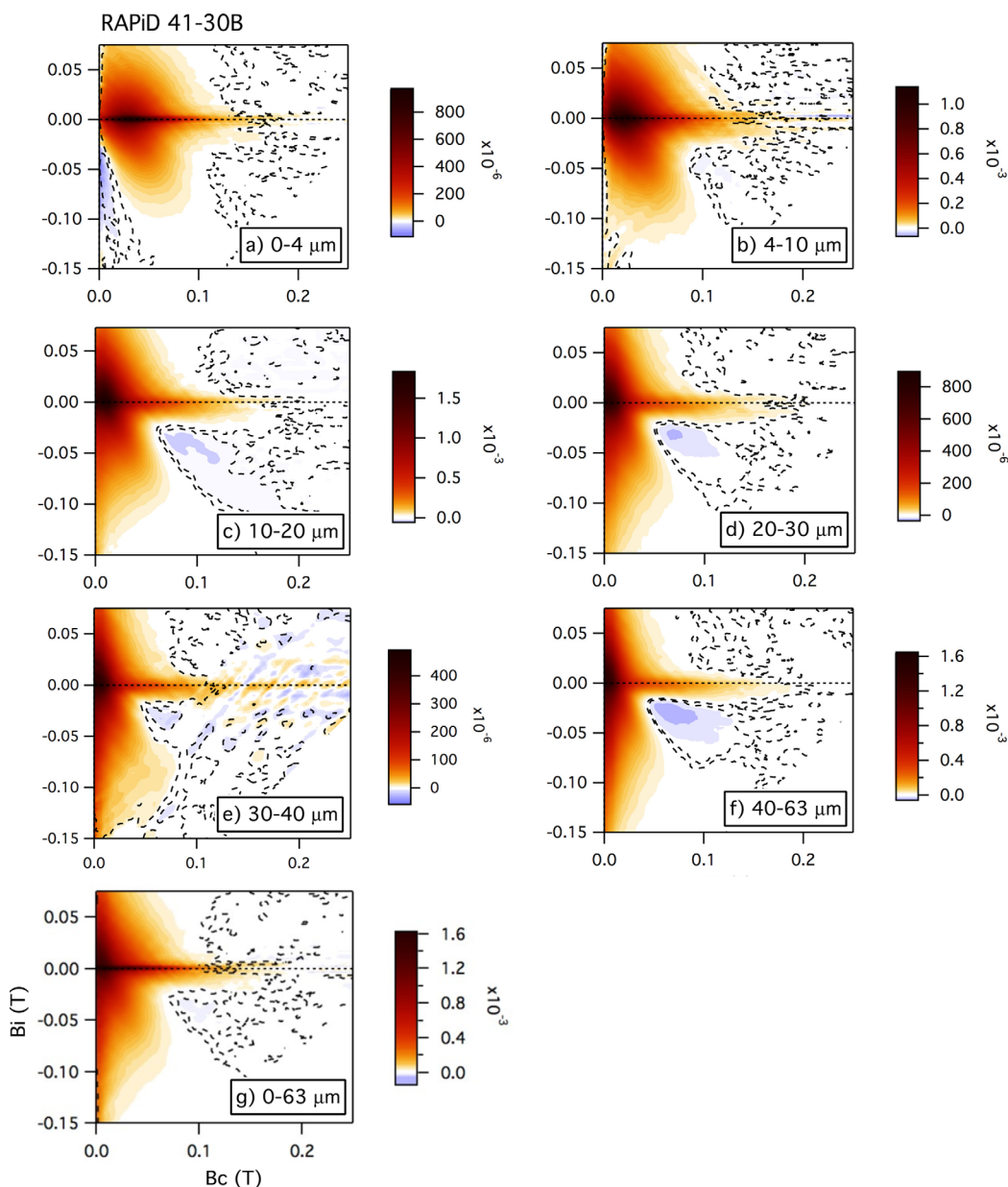


Figure 5. (a–f) FORC diagrams of individual particle size fractions and (g) unseparated treated sediment from Newfoundland-proximal core R41.

and the development of a negative region right of the lobe all indicate a coarsening of the PSD grains in the fine silt fractions (Figures 4b and 4c). The coarsening trend continues in the medium and coarse silt fractions, which are dominated by MD grains (characterized by lower coercivities and pronounced vertical spread). The hematite contribution decreases gradually from the clay fraction, which has the highest concentration, to the fine and medium silt fractions, to being virtually absent in the coarsest silt fraction (Figures 4a–4f).

Core R41, located east of Newfoundland, has the coarsest bulk signature and does not contain any hematite (Figure 5g). The 0–4 and 4–10  $\mu\text{m}$  fractions are dominated by PSD grains (Figures 5a and 5b), while the other fractions (Figures 5c–5f) are notably MD like (very low peak coercivity, wide v-shaped contours, well-expressed negative region right of lobe). The clay fraction exhibits a central ridge and negative region along the vertical axis indicating the presence of SD particles (Figure 5a). The central ridge is also expressed in the unseparated sediment (Figure 5g).



### 3.2. PCA and Unmixing

#### 3.2.1. Binary Mixtures

Both Rockall Trough and Iberian Margin data sets can be described as mixtures of two EMs. We use the Rockall Trough series to demonstrate the choice of EMs for a binary mixing model, as well as to compare the result of the PCA-based unmixing to quantitative unmixing using the central-ridge extraction method [Egli *et al.*, 2010]. For the Iberian Margin series, we analyze the data using two different sampling resolutions for the PCA grids to show that the PCA unmixing method yields similar quantitative results.

##### 3.2.1.1. Rockall Trough

The variability in the Rockall Trough data set is mainly accounted for by PC 1 (Figure 6), which explains 70% of the data variability. PC 2, which explains 4% of the variability, and PC 3, which explains 3% of the variability, are dominated by measurement noise. The series can be modeled as a binary mixture, with one EM being a noninteracting uniaxial SD component (EM1, Figures 6a and 6b), and the other a coarse PSD/fine MD component (EM2, Figures 6a and 6b). The EMs were chosen by moving along PC 1 outward from the limits of the data set to the points where the model FORC diagrams of the EMs appeared to be composed mostly of a single component, and beyond which they became unrealistic physically (Figure 6b). Unphysical FORCs are recognized by the appearance of negative signals in regions of the FORC space not predicted by physical modeling [Harrison and Lascau, 2014]. In this case, PC 1 scores of  $-0.048$  and  $0.0135$  provide EMs that satisfy these criteria. The PSD EM represents the detrital background sedimentation in the Rockall Trough, which appears to be decreasing in abundance upward across the Late Glacial. The SD EM displays all the diagnostic FORC signatures of noninteracting uniaxial SD grains, including a well-defined central ridge and antisymmetric background signals about the  $-45^\circ$  remanence diagonal [Newell, 2005; Egli *et al.*, 2010; Ludwig *et al.*, 2013]. These features are consistent with the presence of intact chains of bacterial magnetosomes [Egli *et al.*, 2010; Li *et al.*, 2012; Harrison and Lascau, 2014]. The presence of individual magnetosomes and partial chains was confirmed by transmission electron microscopy (TEM) of magnetic extracts. The PSD EM fraction is plotted in Figure 6c, along with an analogous curve obtained by computing the fraction of the background signal in the FORC diagrams, after extracting the central ridge using FORCinel [Harrison and Feinberg, 2008]. The two curves are very similar with respect to the direction of variability, but there are slight differences in their relative amplitudes. These discrepancies should be expected because of the different unmixing methodologies, which employ differing EMs (i.e., in the ridge extraction method, one EM is the extracted central ridge, while the other is the background signal, which incorporates both SD and PSD signatures).

##### 3.2.1.2. Iberian Margin

In the Iberian Margin data set, PC 1 explains 72% of the variability if the data are resampled at 5 mT resolution (Figure 7a), and 68% of the variability if the data are resampled at 2 mT resolution (Figure 7b). Higher rank PCs describe only a few percent of the variability and account mainly for measurement noise. Thus, this series can also be modeled as a binary mixture. The model EMs are a fine PSD component (Figures 7a and 7b, insets on left), which reflects distal sedimentation of fine detrital magnetite from the Iberian Peninsula, and a weakly interacting SD component (Figures 7a and 7b, insets on right), representing magnetosomes [Channell *et al.*, 2013]. Even though qualitatively the FORC diagrams from the Iberian Margin cores show only subtle variations between samples, PCA is adept in discriminating between the EMs, albeit not as clear-cut as in the Rockall Trough case. For example, the PSD EM retains a small central ridge signal, while the SD EM contains a vestigial PSD signature above the horizontal axis (insets in Figures 7a and 7b). The results generated via the 5 and 2 mT resolution models are quantitatively comparable: Figure 7c shows there is a 1:1 relationship between the proportions of the PSD EMs obtained from the two models, confirming that sampling resolution is not a crucial factor in quantifying the EM contributions.

#### 3.2.2. Ternary Mixtures

##### 3.2.2.1. Combined Rockall Trough and Iberian Margin Data Sets

The Rockall Trough and Iberian Margin data sets both contain an EM that is representative for magnetosomes. The only constraint imposed in choosing the PC 1 score for this EM was that the FORC diagram be physically realistic, and, where possible, comprise the signature of only one domain state. A further constraint can be imposed by combining the two data sets in the same PCA. The resulting score plot shows that two PCs explain most of the variability in the data set (Figure 8a). The bulk of the data variability is explained by PC 1 (87%), while PC 2 explains 9% of the variability. The two series appear as distinct linear trends that converge to the same point (EM3 in Figure 8a) on the fine-grained end of the data sets. At the coarse-grained ends of the trends, we found two EMs using the same criteria employed for the binary mixtures: a coarse PSD/fine MD EM and a fine PSD EM (EM1 and EM2, respectively, in Figure 8a), which resemble closely, but are not identical



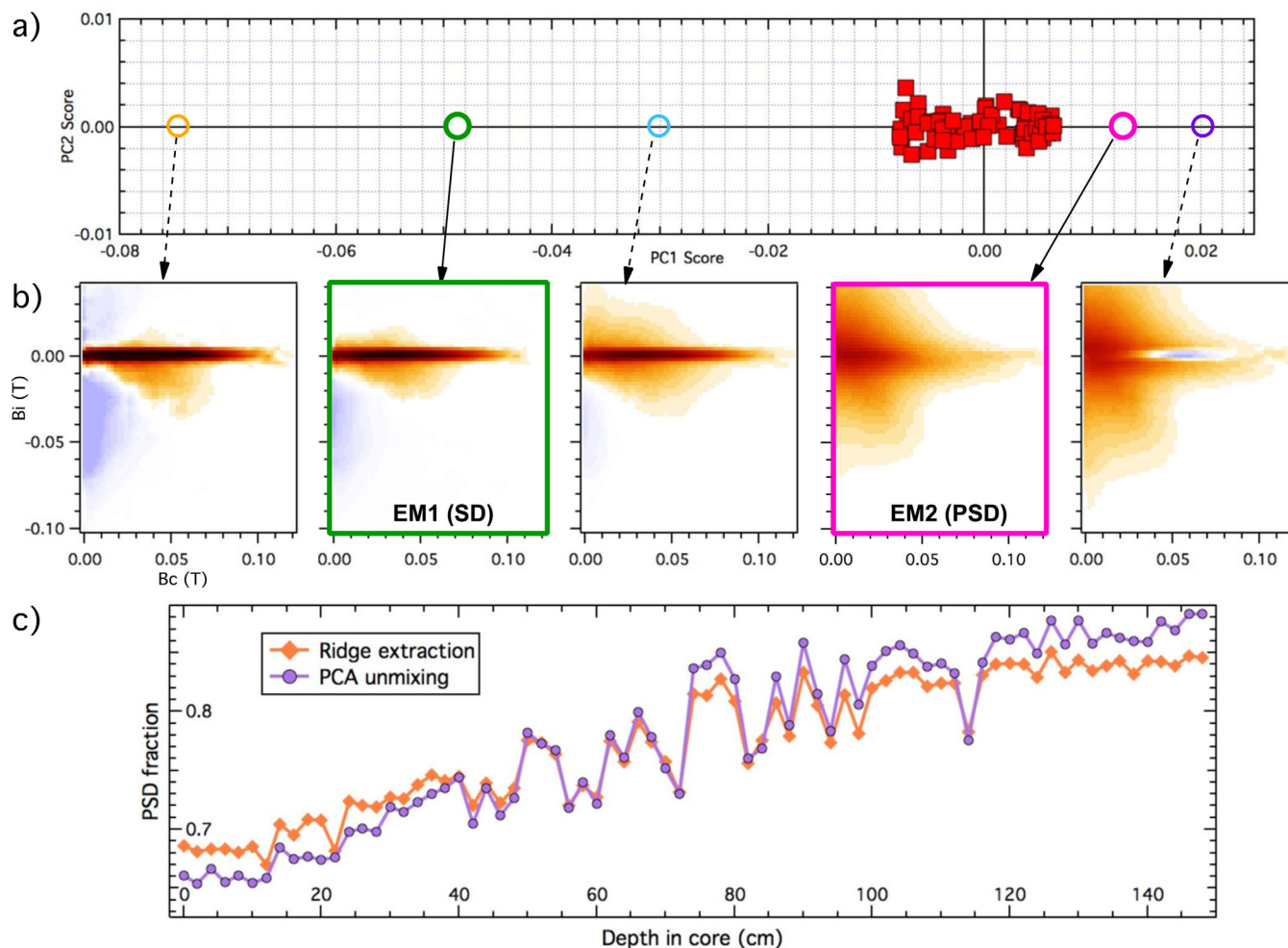


**Figure 6.** (a) PCA score plot of Rockall Trough samples (red squares) with FORC diagrams resampled on 2 mT resolution grids. The larger circles represent the end-members (EMs) used in the binary mixing model, while the smaller circles are compositions that failed the EM selection criteria. (b) Model FORC diagrams of EM1, EM2, and of three failed EM candidates. FORC diagrams of EM candidates with scores lying outside the interval defined by EM1 and EM2 contain physically unrealistic features (outer panels), while those of potential EMs with scores within the interval are not single component FORC distributions (middle panel). (c) Plots of PSD fractional contribution obtained from both PCA (dots) and central ridge extraction (diamonds) methods.

to the coarse-grained EMs calculated in the previous models (Figures 6 and 7). This is explained by different sedimentation regimes in the two depositional environments: the Rockall Trough core is proximal to a glaciogenic submarine fan that received coarser-grained sediment in a shallower setting at the Pleistocene/Holocene transition, while the Iberian Margin samples are located on the distal continental shelf and subject to presently accumulating fine pelagic sediment. The three EMs constitute the vertices of a simplex that encompasses all the data points [Heslop and Roberts, 2012a], which we use as mixing space for a ternary unmixing model. The proportions of the EMs calculated via this model are shown in Figure 8b. The ternary diagram shows that EM3 contributes between 10 and 30% of the FORC signal, values similar to those resulting from the binary unmixing models. The fact that the SD EM is common to both data sets constitutes further evidence for the ubiquitous nature of magnetosomes in marine sediments [Roberts et al., 2012].

### 3.2.2.2. RAPID Cores

PCA of the RAPID core samples yields two PCs that together describe 91% of the variability in the data set (PC 1 accounts for 64% of the variability). The data can be described in terms of three EMs, which were chosen according to the criteria outlined above. To aid in the EM selection, we have included FORC diagrams for two synthetic magnetite samples, a PSD specimen (Wright Co. 3006,  $1.0 \pm 0.7 \mu\text{m}$ ), and an MD specimen (Wright Co. 41183,  $20 \pm 12 \mu\text{m}$ ). The EMs define a mixing space (Figure 9a) that encompasses all the data points but one (R10, 40–63  $\mu\text{m}$ ), which was treated as an outlier due to the large RMS of its residual FORC diagram. EM1 is MD, EM2 is PSD, and EM3 comprises both SD magnetite and hematite signatures (Figure

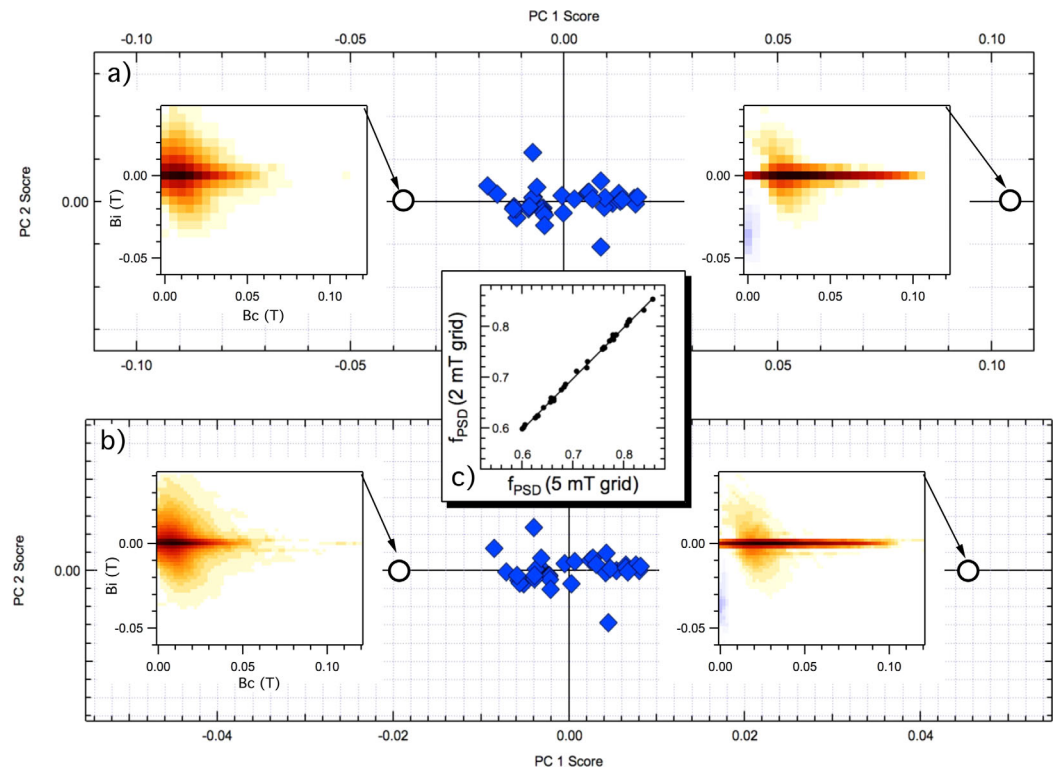


**Figure 7.** PCA score plots of Iberian Margin samples (blue diamonds) with FORC diagrams resampled on (a) 5 mT resolution grids and (b) 2 mT resolution grids. The circles represent the EMs used in the binary mixing model used for quantifying the data. Insets depict model PSD (left) and SD (right) EM FORC diagrams. (c) Biplot showing 1:1 relationship between PSD fractions obtained from the unmixing models in Figures 7a and 7b.

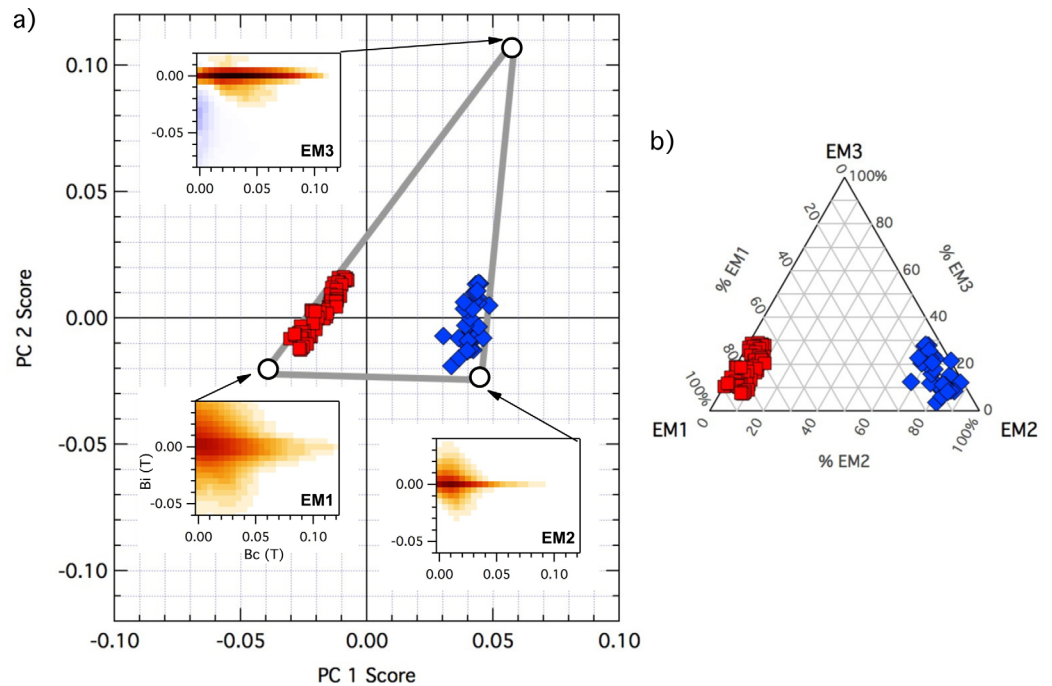


**Figure 8.** (a) PCA score plot of the combined Rockall Trough (red squares) and Iberian Margin (blue diamonds) data sets resampled on 5 mT resolution grids. The three-EM (circles) mixing model shows that both data sets converge to a common EM. Insets depict model EM FORC diagrams for the coarse PSD, fine PSD, and SD EMs (EM1, EM2, and EM3, respectively). (b) Ternary diagram showing relative abundances of the three EMs in each sample.

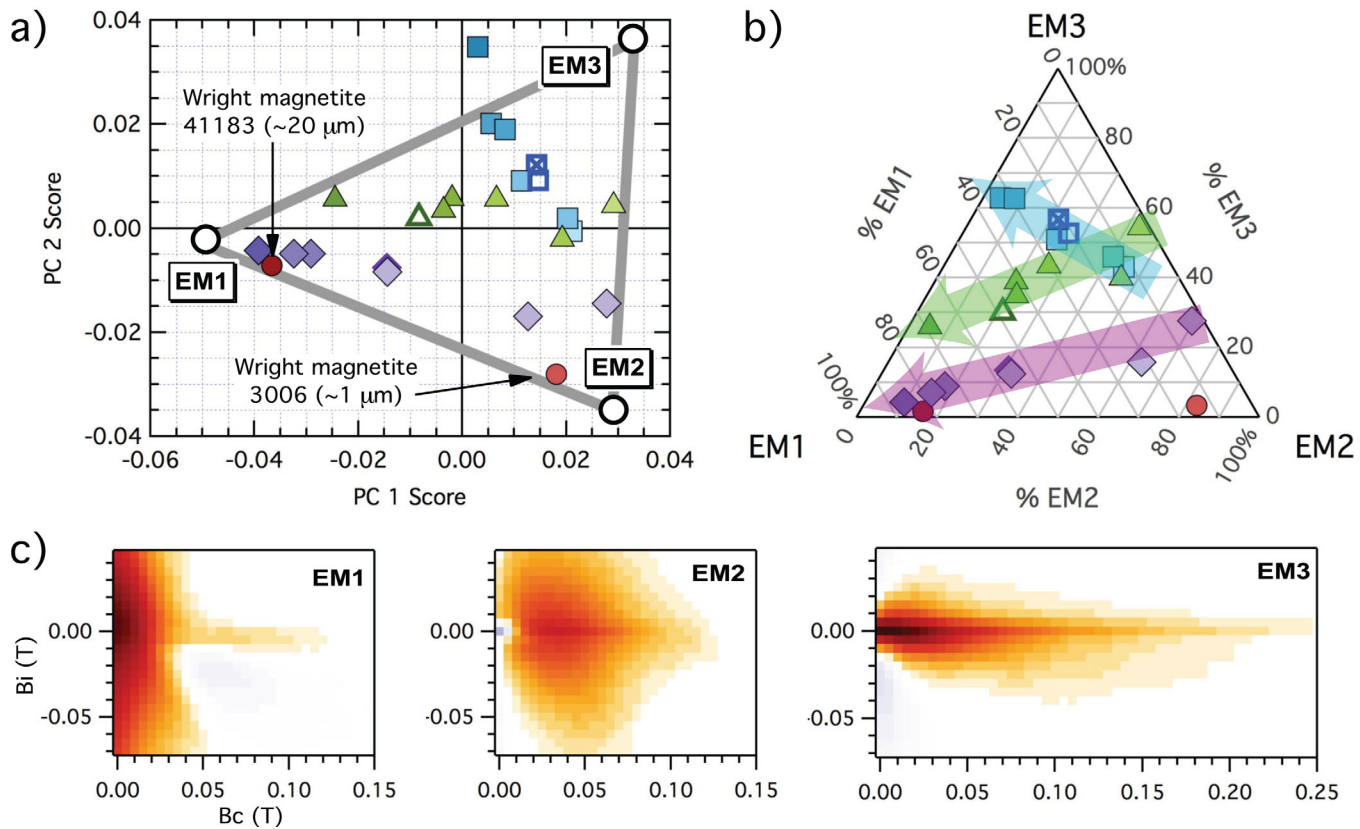


**Figure 9.** (a) PCA score plot of particle size fractions from RAPID cores R10 (blue squares, Iceland-proximal), R29 (green triangles, Greenland-proximal), and R41 (purple diamonds, Newfoundland-proximal), and of Wright Co. synthetic magnetites resampled on 5 mT resolution grids. Full symbols are the individual particle size fractions, with darker colors representing coarser fractions. Open symbols signify the unseparated treated sediment, while the crossed square is the bulk untreated core top sample from R10. Larger open circles represent the EMs of the ternary mixing model employed for quantifying the data. (b) Ternary diagram showing relative abundances of the three EMs in each sample. Note that outlier in Figure 9a is not included in the unmixing analysis. Arrows indicate mixture trends in each core top with increasing granulometric fraction. (c) Computed FORC diagrams of EM1 (MD magnetite), EM2 (PSD magnetite), and EM3 (mixture of SD magnetite and hematite).

9c). Including the outlier in the mixing space would have resulted in EM3 having unphysical features. EM1 is very similar to the coarsest size fraction of core R41, and not far off from the synthetic MD magnetite in the PC score plot, while EM2 is akin to the synthetic PSD magnetite. EM3 has mixed characteristics because it is controlled by the FORC signatures of the clay-sized fractions, which include both SD and fine PSD magnetite grains, as well as hematite. The proportion of each EM in the RAPID samples can be seen in Figure 9b. The ternary diagram shows the samples from each core lying on distinct trends. The bulk samples have similar proportions to the 10–20 μm silts in the case of R10 and R41 and to the 30–40 μm silts in the case of R29. The Iceland-proximal samples (core R10) are mainly mixtures of fine-grained magnetite and hematite (~40–60% EM3). As grain size increases, the proportion of EM2 decreases, with both EM1 and EM3 proportions increasing. The large amount of EM3 in the coarser silts can be explained by the presence of fine-grained magnetite inclusions in silicate grains and/or hematite coatings of large silt particles [Hatfield *et al.*, 2013]. These fine grains are not physically separable from the coarser detrital grains [Hatfield, 2014]. The samples from the cores proximal to Greenland (R29) and Newfoundland (R41) lie on approximately parallel trends and exhibit increasing EM1 proportions with increasing grain size. R29 contains a more important EM3 contribution than R41, suggesting that EM3 fraction represented by inclusions or coatings is being advected with fine and medium silts along the DWBC from areas proximal to Iceland, and progressively removed from the current by sedimentation with increasing distance from its source.

### 3.2.3. Quaternary Mixture

Finally, we demonstrate the power of PCA-based unmixing of FORC diagrams by showcasing the example of a higher-order mixture. PCA performed on the RAPID data set could not readily discriminate between SD magnetite and hematite. Applying PCA to the combined RAPID and Rockall Trough data sets produces three PCs, which collectively explain 91% of the variability in the data set (PC 1 accounts for 68%, PC 2 for



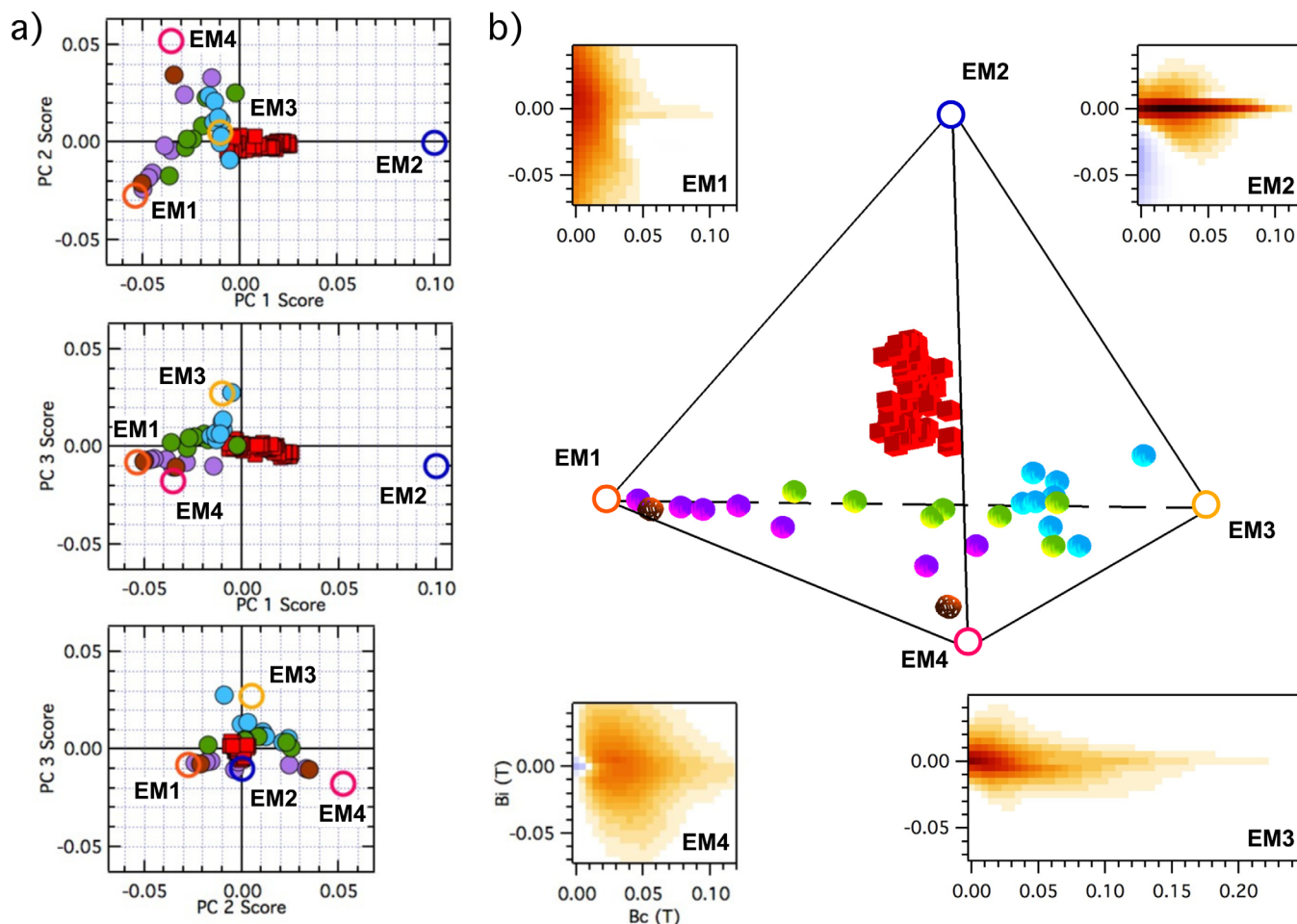


**Figure 10.** (a) PCA score plots of samples from RAPId cores R10 samples (blue circles), R29 (green circles), and R41 (purple circles), Rockall Trough core MD04–2822 (red squares), and Wright Co. magnetites (brown circles) resampled on 5 mT resolution grids. The combination of pairs of PCs in the three biplots illustrates the full spatial relations between the analyzed data points. The open circles represent the EMs of the quaternary mixing model used for quantifying the data. One outlier (same sample as in Figure 9) can be seen in the PC 3 versus PC 2 score plot (with highest PC 3 score). (b) Quaternary diagram showing the proportions of the four EMs in each sample, and computed FORC diagrams of EM1 (MD magnetite), EM2 (SD magnetite), EM3 (mixture of hematite and fine PSD magnetite), and EM4 (PSD magnetite).

18%, and PC 3 for 5%). The three-dimensional score space (Figure 10a and Movie S1) illustrates how the Rockall Trough data set does not lie in the same plane as the RAPId data set, but is oriented almost normal to this plane, with the SD-rich Holocene samples at the distal end of the series. The collective data can be described in terms of four EMs (Figure 10b), with three of them similar to the ones described in the previous section (Figure 9) and one markedly SD in nature. EM1 is MD, EM4 is PSD, EM3 is a mix of hematite and fine PSD magnetite (note the absence of definitive SD features compared to EM3 of the RAPId ternary model), and EM2 is SD, but less clear-cut noninteracting than in the binary mixture case (Figure 6). In general, the EMs are less constrained than in the binary and ternary cases due to the scarcity of data points, which span only a limited region of the three-dimensional simplex defining the mixing space. The quaternary diagram (Figure 10b and Movie S2) excludes one outlier, R10 40–63  $\mu\text{m}$ , the same data point as in the previous model, which has a large residual RMS error. The quaternary mixing model suggests that hematite is preponderant in EM3 of the RAPId ternary mixing model, to the detriment of SD magnetite, and/or that the SD component of the RAPId data set comprises a combination of biogenic and lithogenic particles.

## 4. Discussion

### 4.1. Choice of End-Members

A key feature of PCA is that the PC scores and loading vectors are derived purely on the basis of the natural variations contained within the data set, without the need for subjective user input. This is a powerful

advantage over other FORC quantification approaches (e.g., central ridge extraction), which require case-specific curve fitting of analytical expressions for each EM. The interpretation of the resulting PC space is, however, subjective within a given geological context, and the selection process of the EMs is conducted in supervised fashion. In principle, any combination of  $n + 1$  EMs that fully enclose the sample scores can be used as the basis for unmixing. Our aim is to choose EMs that reflect the true physical components of the system. FORC diagrams of natural samples have been studied extensively over the past 15 years, and a comprehensive knowledge of the range of FORC signatures associated with physically plausible EMs has been accumulated [Pike et al., 1999; Roberts et al., 2000; Carvallo et al., 2003; Muxworthy et al., 2005; Muxworthy and Williams, 2005; Newell, 2005; Egli, 2006; Chen et al., 2007; Egli et al., 2010; Church et al., 2011; Roberts et al., 2014]. Combined with strict constraints on the geometry of FORC diagrams provided by physical modeling [Harrison and Lascu, 2014], it is possible to reduce the subjectivity of EM choice. The choice of EMs becomes even less subjective when there is sufficient variation within the data set to fully define the bounds of the mixing space. The granulometric separation approach adopted here is particularly useful in this context, as it dramatically expands the sampling of the mixing space when the number of bulk samples in the suite is small. Combining data sets and including standard FORC diagrams from well-characterized samples also helps in defining and/or confirming the choice of EMs. The more samples of a given class (e.g., marine sediments in this case) that can be combined in a global analysis, the more accurate and detailed the unmixing will become. This points to a potentially generalized approach to magnetic unmixing, whereby individual samples are projected onto a framework of loading vectors derived from suites of optimized reference FORC diagrams.

The approach adopted here is akin to another multivariate statistical technique, factor analysis (FA), but with the ability to impose constraints on the EMs [Valder et al., 2012], which is critical in the case of FORC diagrams. Like PCA, FA allows a reduction in the number of variables that describe the system, and the identification of new variables (factors) that contain the underlying common structure of the original variables [Mellinger, 1987; Grande et al., 1996; Woocay and Walton, 2008]. However, in FA, the common structure in the data set is hypothesized [Temple, 1978], and unlike PCA, the method directly provides the set of EMs of the system (i.e., the factors). The major caveat of FA is that the resulting EMs do not necessarily represent physically plausible FORC signatures. Post-FA factor optimization methods do not guarantee realistic FORC geometries for the EMs either. Although outside the scope of this initial proof-of-concept study, the use of methods such as Independent Component Analysis (ICA) [Hyvärinen, 1999] may provide a more objective solution to defining the EMs of the system. Combined with image preprocessing, ICA is now routinely used in electron microscopy to perform blind source separation for spectral images [De la Peña et al., 2011]. Along with the envisaged development of libraries containing suites of reference FORCs, ICA presents particular promise in the quest to automatically identify realistic EMs (or at minimum provide initial estimates) for FORC unmixing.

#### 4.2. Physical Meaning of the Mixing Proportions

The FORC diagrams input into the PCA, as well as the ones calculated from equation (2), are normalized to the sum of their values (equation (1)), which is approximately equivalent to normalizing with respect to the double integral of the FORC diagram. In an ideal case (i.e., where only irreversible process contribute to the magnetization), the integral of a FORC diagram is equal to the saturation magnetization,  $M_s$ , enabling  $f_i^l$  to be simply related to the mass or volume fractions of the corresponding EMs. In the general case, however, the integral of a FORC diagram is equal only to the irreversible component of magnetization,  $M_{irs}$ , where  $0 < M_{irs} \leq M_s$ . This is because purely reversible contributions to the magnetization disappear when calculating the mixed double derivative of  $M$  [Pike, 2003]. Converting  $f_i^l$  into mass or volume fractions then requires some knowledge of the relative contributions of reversible and irreversible magnetization to the total magnetization of each EM. If the EMs are physically accessible, then  $M_{irs}/M_s$  can be calculated directly from the experimental FORC diagram. For EMs derived purely from the PCA procedure, however, this quantity is not accessible directly and would have to be estimated from simulations or measurements of analogue systems. Differences between the unmixing proportions derived from PCA and those based on mass or volume fractions are anticipated to be greatest when EMs have very different values of  $M_{irs}/M_s$  (e.g., SP versus SD, or SD versus MD). To circumvent this issue, one can perform the PCA-based analysis directly on the measured magnetization curves, or include the reversible ridge [Pike, 2003] in the analysis. This approach would present the advantage of accounting for both irreversible and reversible contributions to the magnetization. However, its major disadvantage would be the inability to interactively explore the PC space for the purpose of visualizing and selecting EMs. In the included software (see supporting information), the user is able to move a cursor to



any point in the score plot and the corresponding FORC diagram is calculated instantly. This would not be possible if the raw magnetization was used to construct the score plot. The approach we opted for here (i.e., using the mixed second derivative of the magnetization) makes it possible to bring into sharp contrast the characteristic features of different domain states, which is the principal reason FORC diagrams are utilized.

## 5. Conclusions

The ability to break down the magnetic mineralogy of a natural sample into its constituent components is a common task in rock magnetism, as evidenced by the ubiquity of the “Day plot” in the rock magnetism literature. FORC diagrams are sensitive to mineralogy, anisotropy, coercivity, domain state, interactions, and ensemble geometry, and are capable, therefore, of providing good discrimination between different physical components of the system. We have demonstrated that using entire FORC diagrams as the basis for magnetic unmixing has the potential to provide a general route to quantifying multicomponent mixtures. PCA exploits the natural variability contained within the sample suite and allows the analysis to proceed without user input or bias in the initial step. The physical constraints imposed on the EMs preclude the need to perform case-specific least squares fitting to optimize individual EMs. For this reason, the method lends itself readily to automation and can be easily incorporated into existing FORC processing packages (see supporting information). Interpretation of the resulting PC scores is subjective within a geological context, and EM selection is supervised, but this subjectivity can be minimized by including constraints from granulometric filtering, physical modeling, additional data sets or standard reference FORCs. In its current form, unmixing is performed using sum-normalized FORCs that are sensitive to the irreversible component of magnetization only. Alternative procedures will be explored as the method is developed further. Case studies representing binary, ternary, and quaternary mixtures demonstrate that spatial and temporal variations in magnetic mineralogy can be quantified through both intra and intercore comparisons. The method works best when the sample suite covers a large region of mixing space. However, even when the variability is limited, PCA still does a reasonable job of revealing the nature of the EMs. Although initially designed with sediments in mind, the method presented here can equally be applied to suites of igneous, metamorphic, or meteoritic rocks, as well as to synthetic materials.

## Acknowledgments

The data and code used in this paper are available as supporting information and by contacting the authors directly. The research leading to these results has received funding from the European Research Council under the European Union's Seventh Framework Programme (FP/2007–2013)/ERC grant agreement 320750. We thank David Heslop for a constructive review, and an anonymous referee for useful comments on the subject of multivariate statistics.

## References

- Abdi, H., and L. J. Williams (2010), Principal component analysis, *WIREs Comput. Stat.*, 2(4), 433–459, doi:10.1002/wics.101.
- Carvallo, C., A. R. Muxworthy, D. J. Dunlop, and W. Williams (2003), Micromagnetic modeling of first-order reversal curve (FORC) diagrams for single-domain and pseudo-single-domain magnetite, *Earth Planet. Sci. Lett.*, 213(3–4), 375–390, doi:10.1016/S0012-821X(03)00320-0.
- Channell, J., D. Hodell, V. Margari, L. Skinner, P. Tzedakis, and M. Kesler (2013), Biogenic magnetite, detrital hematite, and relative paleointensity in Quaternary sediments from the Southwest Iberian Margin, *Earth Planet. Sci. Lett.*, 376, 99–109, doi:10.1016/j.epsl.2013.06.026.
- Chen, A. P., R. Egli and B. M. Moskowitz (2007), First-order reversal curve (FORC) diagrams of natural and cultured biogenic magnetic particles, *J. Geophys. Res.*, 112, B08S90, doi:10.1029/2006JB004575.
- Church, N., J. M. Feinberg, and R. Harrison (2011), Low-temperature domain wall pinning in titanomagnetite: Quantitative modeling of multidomain first-order reversal curve diagrams and AC susceptibility, *Geochem. Geophys. Geosyst.*, 12, Q07Z27, doi:10.1029/2011GC003538.
- De la Peña, F., M.-H. Berger, J.-F. Hochepeid, F. Dynys, O. Stephan, and M. Walls (2011), Mapping titanium and tin oxide phases using EELS: An application of independent component analysis, *Ultramicroscopy*, 111(2), 169–176, doi:10.1016/j.ultramic.2010.10.001.
- Dunlop, D. J., and B. Carter-Stiglitz (2006), Day plots of mixtures of superparamagnetic, single-domain, pseudosingle-domain, and multidomain magnetites, *J. Geophys. Res.*, 111, B12S09, doi:10.1029/2006JB004499.
- Egli, R. (2004), Characterization of individual rock magnetic components by analysis of remanence curves, 1. Unmixing natural sediments, *Stud. Geophys. Geod.*, 48(2), 391–446, doi:10.1023/B:SGEG.0000020839.45304.6d.
- Egli, R. (2006), Theoretical aspects of dipolar interactions and their appearance in first-order reversal curves of thermally activated single-domain particles, *J. Geophys. Res.*, 111, B12S17, doi:10.1029/2006JB004567.
- Egli, R. (2013), VARIFORC: An optimized protocol for calculating non-regular first-order reversal curve (FORC) diagrams, *Global Planet. Change*, 110, 302–320, doi:10.1016/j.gloplacha.2013.08.003.
- Egli, R., A. P. Chen, M. Winklhofer, K. P. Kodama, and C.-S. Horng (2010), Detection of noninteracting single domain particles using first-order reversal curve diagrams, *Geochem. Geophys. Geosyst.*, 11, Q01Z11, doi:10.1029/2009GC002916.
- Grande, J. A., A. González, R. Beltrán, and D. Sánchez-Rodas (1996), Application of factor analysis to the study of contamination in the aquifer system of Ayamonte-Huelva (Spain), *Ground Water*, 34(1), 155–161, doi:10.1111/j.1745-6584.1996.tb01875.x.
- Harrison, R. J., and J. M. Feinberg (2008), FORCinel: An improved algorithm for calculating first-order reversal curve distributions using locally weighted regression smoothing, *Geochem. Geophys. Geosyst.*, 9, Q05016, doi:10.1029/2008GC001987.
- Harrison, R. J., and I. Lascu (2014), FORCulator: A micromagnetic tool for simulating first-order reversal curve diagrams, *Geochem. Geophys. Geosyst.*, 15, 4671–4691, doi:10.1002/2014GC005582.
- Hatfield, R. (2014), Particle size-specific magnetic measurements as a tool for enhancing our understanding of the bulk magnetic properties of sediments, *Minerals*, 4(4), 758–787, doi:10.3390/min4040758.
- Hatfield, R. G., J. S. Stoner, A. E. Carlson, A. V. Reyes, and B. A. Housen (2013), Source as a controlling factor on the quality and interpretation of sediment magnetic records from the northern North Atlantic, *Earth Planet. Sci. Lett.*, 368, 69–77, doi:10.1016/j.epsl.2013.03.001.

- Heslop, D. (2015), Numerical strategies for magnetic mineral unmixing, *Earth Sci. Rev.*, *150*, 256–284, doi:10.1016/j.earscirev.2015.07.007.
- Heslop, D. and M. Dillon (2007), Unmixing magnetic remanence curves without a priori knowledge, *Geophys. J. Int.*, *170*(2), 556–566, doi:10.1111/j.1365-246X.2007.03432.x.
- Heslop, D. and A. P. Roberts (2012a), A method for unmixing magnetic hysteresis loops, *J. Geophys. Res.*, *117*, B03103, doi:10.1029/2011JB008859.
- Heslop, D. and A. P. Roberts (2012b), Estimating best fit binary mixing lines in the Day plot, *J. Geophys. Res.*, *117*, B01101, doi:10.1029/2011JB008787.
- Heslop, D. and A. P. Roberts (2012c), Estimation of significance levels and confidence intervals for first-order reversal curve distributions, *Geochem. Geophys. Geosyst.*, *13*, Q12Z40, doi:10.1029/2012GC004115.
- Heslop, D., M. J. Dekkers, P. P. Kruiver and I. H. M. Van Oorschot (2002), Analysis of isothermal remanent magnetization acquisition curves using the expectation-maximization algorithm, *Geophys. J. Int.*, *148*, 58–64.
- Heslop, D., A. P. Roberts and L. Chang (2014), Characterizing magnetofossils from first-order reversal curve (FORC) central ridge signatures, *Geochem. Geophys. Geosyst.*, *15*, 2170–2179, doi:10.1002/2014GC005291.
- Hibbert, F. D., W. E. N. Austin, M. J. Leng, and R. W. Gatloff (2010), British Ice Sheet dynamics inferred from North Atlantic ice-rafted debris records spanning the last 175,000 years, *J. Quat. Sci.*, *25*(4), 461–482, doi:10.1002/jqs.1331.
- Hyvärinen, A. (1999), Fast and robust fixed-point algorithms for independent component analysis, *IEEE Trans. Neural Networks*, *10*(3), 626–634, doi:10.1109/72.761722.
- Kruiver, P. P., M. J. Dekkers, and D. Heslop (2001), Quantification of magnetic coercivity components by the analysis of acquisition curves of isothermal remanent magnetisation, *Earth Planet. Sci. Lett.*, *189*, 269–276.
- Lascu, I., S. K. Banerjee, and T. S. Berquó (2010), Quantifying the concentration of ferrimagnetic particles in sediments using rock magnetic methods, *Geochem. Geophys. Geosyst.*, *11*, Q08Z19, doi:10.1029/2010GC003182.
- Li, J., W. Wu, Q. Liu, and Y. Pan (2012), Magnetic anisotropy, magnetostatic interactions and identification of magnetofossils, *Geochem. Geophys. Geosyst.*, *13*, Q10Z51, doi:10.1029/2012GC004384.
- Ludwig, P., R. Egli, S. Bishop, V. Chernenko, T. Frederichs, G. Rugel, S. Merchel, and M. Orgeira (2013), Characterization of primary and secondary magnetite in marine sediment by combining chemical and magnetic unmixing techniques, *Global Planet. Change*, *110*, 321–339, doi:10.1016/j.gloplacha.2013.08.018.
- Malinowski, E. R. (1991), *Factor Analysis in Chemistry*, John Wiley and Sons, New York.
- Mellinger, M. (1987), Multivariate data analysis: Its methods, *Chemometrics Intel. Lab. Syst.*, *2*, 29–36, doi:10.1016/0169-7439(87)80083-7.
- Muxworthy, A., and W. Williams (2005), Magnetostatic interaction fields in first-order-reversal-curve diagrams, *J. Appl. Phys.*, *97*(6), 063905, doi:10.1063/1.1861518.
- Muxworthy, A. R., J. King, and D. Heslop (2005), Assessing the ability of first-order reversal curve (FORC) diagrams to unravel complex magnetic signals, *J. Geophys. Res.*, *110*, B01105, doi:10.1029/2004JB003195.
- Newell, A. J. (2005), A high-precision model of first-order reversal curve (FORC) functions for single-domain ferromagnets with uniaxial anisotropy, *Geochem. Geophys. Geosyst.*, *6*, Q05010, doi:10.1029/2004GC000877.
- Pike, C. R. (2003), First-order reversal-curve diagrams and reversible magnetization, *Phys. Rev. B*, *68*, 104424, doi:10.1103/PhysRevB.68.104424.
- Pike, C. R., A. P. Roberts and K. L. Verosub (1999), Characterizing interactions in fine magnetic particle systems using first order reversal curves, *J. Appl. Phys.*, *85*(9), 6660–6667.
- Roberts, A. P., C. R. Pike, and K. L. Verosub (2000), First-order reversal curve diagrams: A new tool for characterizing the magnetic properties of natural samples, *J. Geophys. Res.*, *105*, 28,461–28,475, doi:10.1029/2000JB900326.
- Roberts, A. P., L. Chang, D. Heslop, F. Florindo and J. C. Larrasoana (2012), Searching for single domain magnetite in the “pseudo-single-domain” sedimentary haystack: Implications of biogenic magnetite preservation for sediment magnetism and relative paleointensity determinations, *J. Geophys. Res.*, *117*, B08104, doi:10.1029/2012JB009412.
- Roberts, A. P., D. Heslop, X. Zhao and C. R. Pike (2014), Understanding fine magnetic particle systems through use of first-order reversal curve diagrams, *Rev. Geophys.*, *52*, 557–602, doi:10.1002/2014RG000462.
- Robertson, D., and D. France (1994), Discrimination of remanence-carrying minerals in mixtures, using isothermal remanent magnetisation acquisition curves, *Phys. Earth Planet. Inter.*, *82*(3–4), 223–234, doi:10.1016/0031-9201(94)90074-4.
- Temple, J. T. (1978), The use of factor analysis in geology, *J. Int. Assoc. Math. Geol.*, *10*(4), 379–387, doi:10.1007/BF01031743.
- Valder, J. F., A. J. Long, A. D. Davis, and S. J. Kenner (2012), Multivariate statistical approach to estimate mixing proportions for unknown end members, *J. Hydrol.*, *460–461*, 65–76, doi:10.1016/j.jhydrol.2012.06.037.
- Wold, S., K. Esbensen, and P. Geladi (1987), Principal component analysis, *Chemometrics Intel. Lab. Syst.*, *2*, 37–52, doi:10.1016/0169-7439(87)80084-9.
- Woocay, A., and J. Walton (2008), Multivariate analyses of water chemistry: Surface and ground water interactions, *Ground Water*, *46*(3), 437–449, doi:10.1111/j.1745-6584.2007.00404.x.